CHALMERS
UNIVERSITY OF TECHNOLOGY

Aero-thermo analysis of a waste heat recovery heat exchanger

Proceedings of the ASME 2025
16-20, 2025, Memphis, Tennessee, USA

GT2025-153194

AERO-THERMO ANALYSIS OF A WASTE HEAT RECOVERY HEAT EXCHANGER

Isak Jonsson[2], Jonas Bredberg[1], Valentin Vikhorev[2], Yasser Alrifai[1], Jonathan Bergh[2]

[1] GKN Aerospace Sweden AB, Trollhättan, SE-46138, Sweden
[2] Chalmers University of Technology, Gothenburg, SE-41296, Sweden

ABSTRACT

This study investigates the aerothermal performance and flow dynamics of a heat recovery heat exchanger for the WET cycle concept. A combined experimental and numerical approach is used to assess how flow turning influences heat transfer and pressure losses. The heat recovery unit comprises a radially distributed tube bank, with a length in excess of two meters, downstream of the turbine exhaust. The tested 30 degree sector, consists of 860 tubes. The selected heat recovery design, with the exhaust gases radially turned 90 degrees and flowing through the tubes, results in a highly non-uniform flow posing significant challenges for accurate performance assessment. The experimental evaluation was conducted at Chalmers University using a 1:1 scale model operating under engine representative conditions. Numerical RANS simulations were performed at GKN Aerospace Sweden using ANSYS Fluent on a computational domain of 65 million cells, with a detailed in-tube model for heat transfer evaluation. The overall aerothermal performance shows good agreement between experimental and numerical results; however, at a detailed level, notable discrepancies are identified. The effect of baffle spacing on flow stability and pressure loss distribution is discussed in detail. This study highlights the potential of the combination of relatively simple experimental configurations in combination with detailed numerical simulations provide insights into non-standard HEX configurations.

Keywords: SWITCH, WET, HEX, HRSG, waste heat recovery

NOMENCLATURE

p	Pressure [Pa]
p_0	Total Pressure [Pa]
T	Temperature [K]
U_q	Voltage for heating [V]
A_q	Current for heating [A]
V	Outlet velocity [m/s]
$\dot{m}$	Mass flow rate [kg/s]
HTC	Heat transfer coefficient $[W/m^2K]$
η_r	Row effectiveness [-]
q	Heat flux per unit length [W/m]
Q	Total heat input [W]
L	Length [m]
$_{in}$	Subscript for inlet
$_{out}$	Subscript for outlet
$_{wall}$	Subscript for wall
ADP	Aero Design Point
HEX	Heat Exchangers
HRSG	Heat Recovery Steam Generator
LES	Large Eddy Simulation
LPT	Low Pressure Turbine
OGV	Outlet Guide Vane
RANS	Reynolds-Averaged Navier-Stokes
SWITCH	Sustainable Water-Injecting Turbofan Comprising Hybrid-Electrics
TRS	Turbine Rear Structure
WET	Water Enhanced Turbofan

1 Introduction

The efficient management of distributing flow through heat exchangers (HEX) remains a critical challenge in the development of sustainable aviation systems. This challenge is particularly

pronounced in systems integrating complex aerodynamic and thermodynamic components, such as hydrogen fuel cells and advanced thermal management solutions. Efforts by projects like NEWAC [1, 2], LEMCOTEC [3, 4], ENABLEH2 [5–7], and MINIMAL highlight the inherent difficulties in achieving flow stability and uniformity while turning the flow upstream or within heat exchangers. These challenges have significant implications for heat transfer, efficiency, system stability, and overall performance.

Despite substantial research into both turning vanes, diffusing duct and HEX pressure losses, the combination has a notable absence of established design guidelines or benchmarks. Turning flow introduces significant non-uniformities and flow instabilities, which often propagate into downstream components causing degraded performance. A downstream HEX can either act to guide the flow or produce an adverse pressure gradient causing early separation. The ability to understand, quantify, and control these phenomena is essential for developing thermal management of the next generation of sustainable aviation systems. This study presents an exploratory investigation into the issue, using a relatively simple but representative experimental and numerical setup. The experimental setup focuses on the interaction of flow turning, heat transfer, and pressure loss within a representative tube bank. By combining high-resolution experimental measurements with numerical simulations, this work aims to provide a deeper understanding of the underlying mechanisms and issues to be addressed in future design approaches. The findings from this study are directly relevant to emerging aerospace technologies related to increasing the thermal efficiency of the engine by recovering the waste heat in the core exhaust, enabled by advanced thermal management cycles. Such cycles are relevant not only for improving fuel burn and emissions from kerosene-burning engines but also in future hydrogen-based propulsion systems, where low future fuel consumption is essential for long-distant flights.

1.1 The WET Cycle

In the 1970s, Cheng patented a gas-turbine cycle which integrated steam injection in the combustor, pre-heated by exhaust gas [8, 9]. This proposed gas turbine cycle recovered the exhaust gas heat to generate steam in what is known as a heat recovery steam generator (HRSG). The cycle was originally termed the Dual Fluid Cycle but evolved into the Cheng cycle, combining elements from the Brayton gas turbine and Rankine steam generation cycles. The adoption of steam-injected gas turbines gained momentum within ground power plants and marine applications, due to the superior power density, enhanced thermal efficiency, and reductions in NO_x emissions. However, despite these advantages, the integration of steam-injected gas turbines into aviation engines posed significant challenges. The project Sustainable Water-Injecting Turbofan Comprising Hybrid-electrics (SWITCH) project investigated the WET cycle. The WET Cycle as shown in Fig. 1 utilizes a combination of vaporizers, condensers, and onboard water reserves to recycle water in the exhaust gas. One of the conclusions from the first phase of the SWITCH project is the challenge of sourcing water with acceptable increase in complexity, weight, and drag. Combining a Cheng cycle with hydrogen has inherit benefits compared to a kerosene burning alternative. Hydrogen generates up to twice as much water for the same specific heating values as Jet-A1 and could provide a compact source for water injection. The HySIITE project, [10], by Pratt & Whitney, aims to do just this and could provide the solution for a substantial improvement in core power density and efficiency for future sustainable aviation.

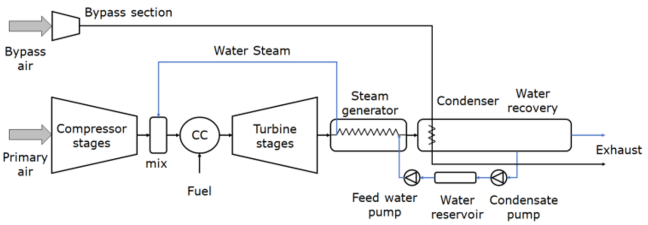

FIGURE 1. Schematic of the SWITCH WET (Water Enhanced Turbofan) engine including the steam generator (vaporizer) component located aft of the gas turbine core (steam turbine not shown) (Reproduced from Stefanizzi et al [11])

Starting with the water downstream of the condenser in Fig. 1, liquid water is pressurized and heated, vaporized and superheated in the steam generator/vaporizer, consisting of a tubular Heat EXchanger (HEX), using energy from the exhaust gas. The high pressure, super heated steam powers a turbine for added mechanical energy. The steam then enters the combustion chamber for wet-combustion, improving power extraction while reducing NO_x emissions. The exhaust gas from the core engine passes through the steam generator and then enters the condenser, cooled using bypass air. The condensation of water, makes the system semi-closed with only limited amount of additional water needed.

1.2 The Vaporizer in SWITCH/WET

The HEX is constructed in sectorial modules, each of 30° angle, making 12 modules to complete the HEX. The vaporizer is mounted on the turbine rear structure (TRS), behind the low pressure turbine (LPT). The exhaust gas is de-swirled through the TRS, guided to the center of the HEX, and then turned 90°, while being distributed throughout the HEX using guide vanes. The gas then passes radially through the axially oriented tubes in a cross-flow arrangement. The water (steam) that flows through

the tubes, in alternative opposite directions, is zigzagging radially inward to the center of the HEX. This arrangement makes the vaporizer a combined cross-flow and a counter-flow HEX design, see Fig. 2. Note that, because of the radial arrangement of the HEX, the flow area increases while the exhaust gas expands, diffusing outward. In summary, this HEX design gives rise to a number of challenging aspects, summarized in the following;

- High speed axial flow, turned 90° radially outwards.
- Even distribution of the flow along the length of the HEX.
- Radially expanding flow through the HEX.

In addition to the above, the HEX is exposed to high temperature and pressure, along with the overarching goal of being lightweight and compact with as little as possible adverse effect on the core engine performance.

The proposed steam generator with one 30° module as shown in Fig. 3 is described here. The active length of the HEX is in excess of two meters. Each module consists of 860 tubes, with varying number of tubes in each row, increasing outwards, see Fig. 4 for details. Each row is staggered in relation to the previous one to enhance flow mixing and heat transfer. The HEX extends, radially, from the outlet of the LPT to roughly twice that diameter. Supporting baffles, are distributed axially along the tube bank to enhance the structural integrity and act as dampers. Elastic analysis of the tubes, using design rules from the VDI handbook, [12], gives a need of 9 supportive baffles, which are consequently added to the design. Guide vanes are attached to the lower part of the baffles that support the redirection of exhaust gases into the HEX. The leading edge of these is located at different radial positions in a staggered fashion, see Fig. 2. The purpose of their extension, in addition to redirect, is also to "shave off" a proportional amount of the flow, ideally 10 % into each of the 10 segments. The flow is gently expanding in the distributing channel to reduce velocity and improve redirection of the flow, although it is well understood that 9 guide vanes, across a distance of more than two meters, are neither sufficient for redirecting the flow, nor to control the flow distribution.

2 Approach

The study focuses on the air-side aerothermal performance of a long vaporizer in the WET cycle. The nominal condition is the Aerodynamic Design Point (ADP), i.e. cruise at altitude, with Reynolds number matched using mass flow scaling in the laboratory 1:1 scale rig. Dry air is used instead of wet exhaust gases to eliminate condensation effects and maintain a controlled thermal environment. This will be tested with less comprehensive instrumentation in another part of the project. Numerically, steady-state RANS simulations were selected to reduce computational cost. Previous analysis revealed that resolving the details, including the 860 tubes, was preferable to reverting to modeling the tube bank as a porous media. The downside of this is that

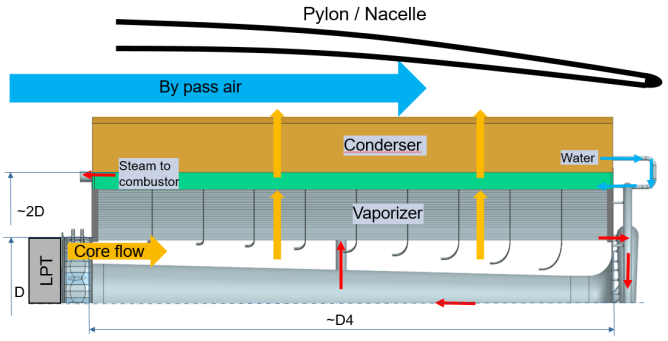

FIGURE 2. An illustration of the installed heat recovery system in the nacell in the SWITCH/WET concept

the computational domain grew to 65 million cells. Experimentally, the long and thin tubes with non-uniform heating provide a substantial challenge for internal local heat transfer and pressure loss measurements. The measurements show the effect of highly non-uniform inlet flow (into a HEX) with corresponding increased pressure loss, as well as providing detailed insights into flow turning and diffusion effects.

3 Experimental Set-up

An isometric view of the 30° sector experimental setup is illustrated in Fig. 3 together with schematic flow field, instrumentation, coordinate system, and sector enumeration which will be referred to throughout this section. The setup has three main access points, traversing the outlet of the tube bank, optical access both from the side (via transparent windows) and at the outlet of the tube bank, and instrumented tubes in the tube bank. The instrumentation for each subsystem is described in this section and data acquisition between and system control is coordinated via Labview shared variables. The module has extended side walls compared to the original design to mitigate interference from flow fields in the room at the outlet. Reynolds number was altered by varying mass flow at the inlet and is deduced by a multiple from ADP, i.e. 2xADP is twice the mass flow as for ADP.

The facility is driven by a FLEBU-B1-315 radial fan and mass flow is measured via an adjustable EKOSI 315 IRIS dampener using an inlet temperature and pressure sensor for density calculations and a PSI-9116 for pressure difference. The inlet conditions are measured in the TRS module via a Prandtl Tube ($p_{0,in}$, p_{in}) and a PT100, model 7304000 from Pentronic AB for inlet temperature (T_{in}). The ambient pressure was measured in the room using the built-in barometer in the Furness control FCO-560 implemented for pressure measurement at the outlet, described later in this work.

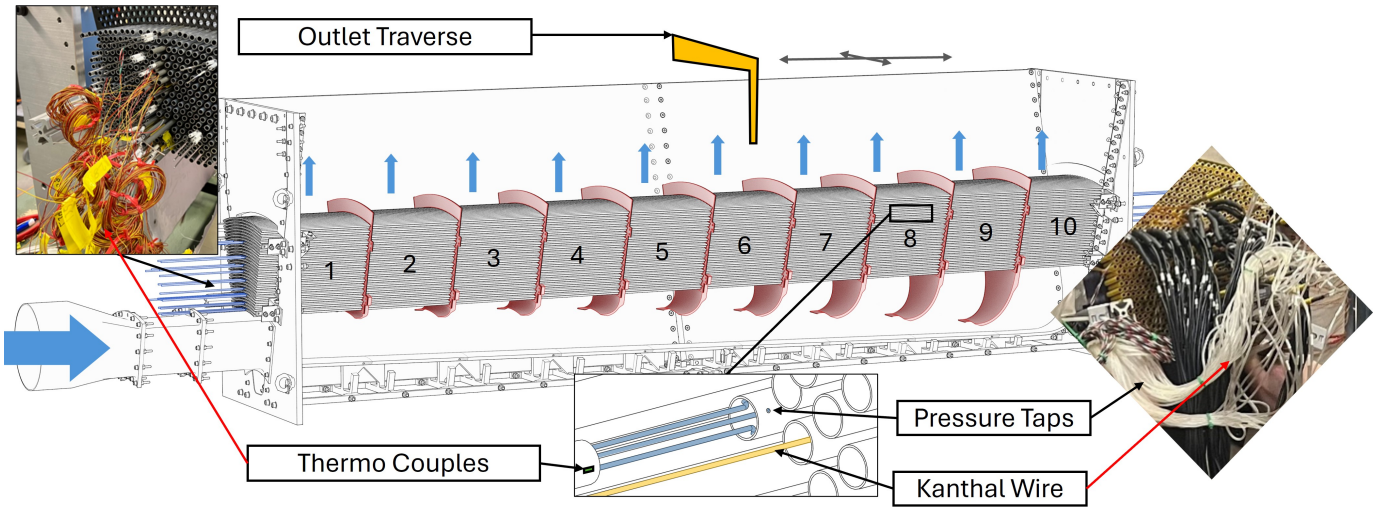

FIGURE 3. Isometric view of the 30° sectional SWITCH/WET vaporizer evaluated at Chalmers with both description and photos of key instrumentation. The air flow is indicated by blue arrows

3.1 Pneumatic Measurements

Aerodynamic evaluation was performed by instrumented tubes in the tube bank with pressure taps and by traversing the outlet of the tube bank with pneumatic probes. In total, 94 pressure taps were located inside the tube bank which were all connected to two Scanivavle revolvers using two ports of the PSI-9116 for data acquisition. A schematic layout of the location of the instrumented tubes is shown in Fig. 4 where the location of the tubes are indexed by row and column number. Individual tubes had several pressure ports. Figure 4 also shows the location of tubes instrumented for heat transfer, later presented in this section.

An ISEL Microstep Controller C142 was used in combination with 2 linear motion axis of model LES-5 to traverse both Prandtl and in-house manufactured Kiel probes at the outlet of the tube bank. If not otherwise specified, all pressure sensors are connected to a PSI-9116 for Pressure Systems with an FSD of 2500Pa. The traversing of sensors allows for a full study of the outlet of the tube bank. A suitable sampling time for downstream measurement was found by cumulative mean convergence for ten random points. Due to the low-speed nature of the application in combination with the relatively large separation, a sampling time of 15s was necessary. With an outlet plane of over 12,000 points, this is a total sampling time of around two days. For low-speed application, the FCO560 was connected to measure the total pressure at the outlet.

3.2 Optical Measurements

A full outlet approach was elected for optical measurements instead of patching several measurement planes together to get a representative flow field average. However, with an active length of the HEX in excess of two meters, and a maximum of 2600

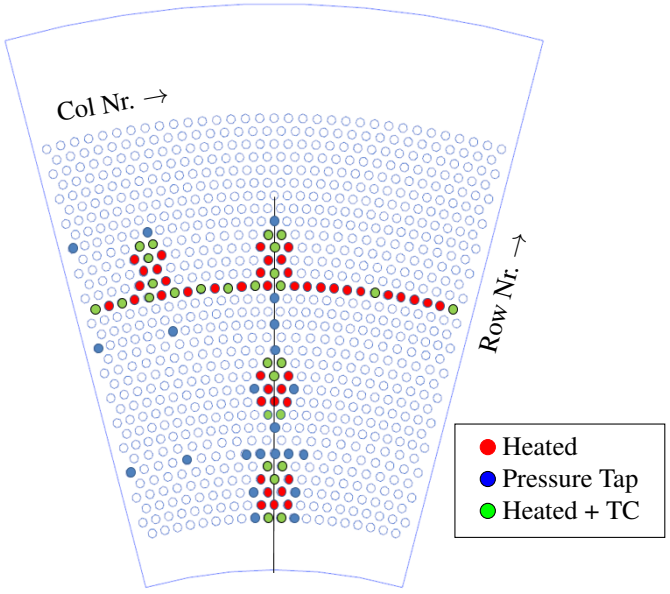

FIGURE 4. Illustration of the tube bank instrumentation with blue circles representing pressure taps, red heated and green with a black circle are heat and instrumented with thermocouple (TC)

pixels with of the Phantom Miro M340 currently available in the lab, individual tracers would need to be in the mm size which is too large to pass through the tube bank, so PIV was not feasible. Hence, the contrast from a rapid introduction of smoke was utilized to trace the flow distribution between the baffles in a single frame. Different processing method was approached but the two most suitable were a simple background removal or a com-

bination of Sobel and Gaussian filters in LaVision Davis 10 software. The approach was similar as applied in Vikorev [13]. This method provides a qualitative comparison of mass flow distribution between the baffles, by repeating the measurement several times a good average could be achieved. A 28-mm f/2.8 Sigma lens was utilized with the Miro M2340 and a light sheet from a slit lamp. The camera viewed the full outlet from the side and at the inlet to the Flebu fan was rapidly saturated with standard glycerine smoke to create a smoke wave. An example processing is shown in Fig. 5.

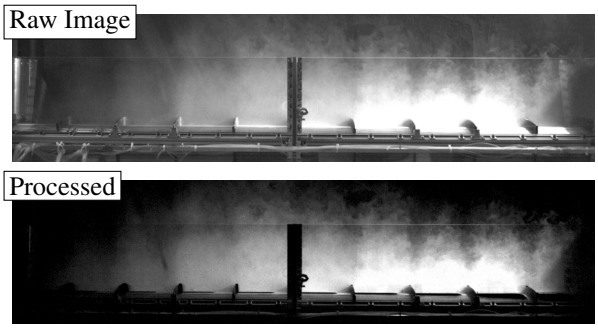

FIGURE 5. A single frame processing history, showing the raw image (top) and processed output (bottom).

3.3 Aerothermal Measurements

A selection of the tubes are instrumented for heat transfer purposes, indicated in Fig. 4 by "Heated" and "Heated + TC". These tubes are heated by Joule heating using an insulated Kanthal wire held suspended in the center by tension. The tubes can be heated individually or as clusters. DC-Power is provided by an EA-PS 3150-04 AC-DC supply where each tube in the cluster is connected in parallel or individually heated to provide uniform power-loss even with a variation of resistance between each tube. The power supply EA-PS 3150-04 AC-DC provides a 1% of uncertainty of the power output. This does not account for the losses in the wiring to the tube bank connector. By adding an accurate current meter and reading the voltage drop across the tube bank the accuracy is better than 1%, this was not implemented in current work however as losses in the cables were estimated to be small.

A selection of the heated tubes has been instrumented with 0.1mm K-type thermocouples (TC) where the surface temperature $T_{wall,i}$ variation can be utilized to assess the uniformity of heat transfer at three different axial and circumferential (clockwise 6, 9 or 3 and 12) positions along individual tubes. The TC is connected to three NI-9213 16 channel 24-bit Data Acquisition (DAQ). Note that experimental temperature and velocities are utilized in the numerical domain so surface temperatures are compared directly instead of calculating the surface heat transfer rate.

3.4 Uncertainty Analysis

Guidelines from ISO 5157 [14] and PTC 19.1 [15] together with numerical simulation have been utilized to estimate the uncertainty via Taylor Expansion and Monte Carlo Simulations (MCS) throughout the experimental work. Accreditation and accuracy provided in data sheets have been utilized if otherwise not specified for individual and derived errors are specified in Table 1.

TABLE 1. Measurement with average individual values at ADP, ie expected uncertainties, and comments. Measurement types are split by horizontal lines and key parameters at ADP are shown last.

Parameter	Avg	ε	Comment
T_{in} [K]	300.00	< 0.07	Pent. PT-100,NI-9217
T_{out} [K]	310.00	< 0.07	Pent. PT-100,NI-9217
$T_{\text{wall,i}}$ [K]	360.00	0.10	K-type TC, NI-9213
p_{amb} [Pa]	101250	0.01%	FCO-560
$p_{0,\text{in}}$ [Pa]	400	0.015%	PSI-9116
$p_{0,\text{out}}$ [Pa]	1	0.15%	FCO-560
p_{wall} [Pa]	300	0.15%	PSI-9116 + Scanivavle
U_q [Volt]	60	2%	EA-PS 3150-04
A_q [Amp]	100	2%	EA-PS 3150-04

3.5 Practical Considerations

Even though this section specifies the instrumentation for the current setup, the authors would like to provide extended comments on the background and considerations from an experimentalist point of view. Joule heating was chosen for this study over traditional techniques, such as water circulation and NTU or heat pipes, due to its simplicity and accuracy. Traditional water circulation would have been arduous to install with thousands of pipe joints and was expected to provide indecisive or at least a very limited operational window for accurate results of both temperature and heat flow. Heat transfer measurements in such systems rely on bulk parameters like mass flow rate and temperature differences. This is especially ill-suited in the current setup with long and thin tubes located in non-uniform flow since no linear or logarithmic temperature development of bulk water temperature can be assumed. Heat pipes were also considered but saturated at the targeted heat flow and the high $L/d = 460$ of the tubes.

Joule heating, on the other hand, ensures a nearly constant heat flux along the tube length independent of ambient conditions and simplifies measurements by using voltage and current readings to calculate heat flow which are substantially less arduous and in general accurate than mass flow and temperature readings. The Kanthal wire's low thermal coefficient of resistance

$(49 \times 10^{-6}\,\mathrm{K}^{-1})$ is key to the consistent heating per unit length. Furthermore, since the wiring is insulated, direct measurement of the tube wall temperature via resistance changes is possible, providing high-resolution insights into localized heat transfer in the bank, this was however not implemented in the current work.

4 Numerical Set-up

The numerical simulations were performed using ANSYS Fluent software, employing a three-dimensional (3D) approach with Reynolds-Averaged Navier-Stokes (RANS) equations and the k-ω Shear Stress Transport (SST) turbulence closure model [16]. A second-order numerical scheme was used for spatial discretization, and the simulations were iteratively progressed in a pseudo-transient manner. The fluid properties were assumed to be constant, with typical values for air at standard conditions, and thermal conductivity. The incompressible governing equations, i.e. the continuity, momentum, and energy equations, are given by;

$$\frac{\partial U_i}{\partial x_i} = 0 \tag{1}$$

$$\rho \frac{DU_i}{Dt} = -\frac{\partial P}{\partial x_i} + \frac{\partial}{\partial x_j}\left(\mu \frac{\partial U_i}{\partial x_j} - \rho \overline{u_i' u_j'}\right) \tag{2}$$

$$\rho \frac{DT}{Dt} = \frac{\partial}{\partial x_i}\left[\frac{\mu}{Pr}\frac{\partial T}{\partial x_i} - \rho \overline{u_i' t}\right] \tag{3}$$

Boundary conditions are set to; mass flow at the inlet and (static) pressure at the outlet, with no-slip conditions at all domain walls and a constant heat-flux at selected heated tubes. The (nominal) mass flow is based on the inlet Reynolds number, given from ADP conditions, i.e. cruise speed at altitude. This gives a low Mach number inlet velocity in the TRS section under standard atmospheric conditions. This translates to an average inlet velocity in the sub-unity in the tube matrix - if uniform flow is achieved. In the CFD simulations, the inlet temperature (T_{in}) and the outlet pressure ($P_{\mathrm{s,out}}$) are both set to standard atmospheric conditions. The CFD results are then linearly shifted to match the measured conditions, which vary depending on atmospheric conditions.

The computational domain was prepared in BETA CAE Systems pre-processor, ANSA, and based on the same CAD model used when constructing the rig, see Fig 6. The baffles, with the attached guide-vanes, were individually measured, after assembly, and then re-positioned in the CFD model. It has previously been shown (during the design process) that the exact location of the guide-vane tip, has a large impact on the mass flow distribution in the tube bank segments. However, it cannot be ascertained that the tip location was identified to a satisfactory level as there is a substantial difference in the predicted and measured mass

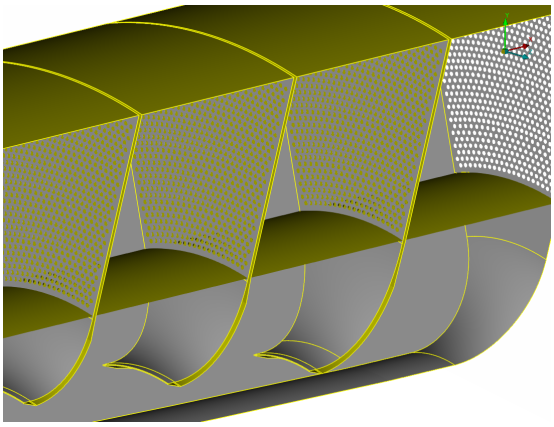

FIGURE 6. Isometric view of the numerical domain showing segments 7-10 with guide vanes, baffles, walls and internal surfaces for sub-division of the domain. Note that the tubes are removed for clarity.

flow distribution in the segments. The computational mesh was predominantly made with hexahedral cells, including five boundary layers. The total amount of cells is 65 million, which makes transient simulation a challenge, although it is advisable for a case characterized by large-scale separation, such as this, to use e.g. LES (Large Eddy Simulations).

Although the Kanthal wire provides a nearly constant heat flux per length unit, the heat flow is redistributed inside the tube before entering the CFD domain. This conjugate heat transfer is unfeasible to fully resolve during the main iterative solution. A sub-model was thus constructed for each tube. In that sub-model, the internal details such as the Kanthal wires, its Teflon insulation, and wall thickness were included. The HTC, as predicted from the main CFD model, was superimposed as a boundary condition into the sub-model from which accurate surface temperatures could be extracted.

5 Results and Discussion

Figure 7 presents the total pressure losses ΔP_t across the steam generator as a function of the dynamic pressure q at the domain inlet. The total pressure losses include contributions from the diffuser, turning baffles, and the tube bank. Experimental data, represented by black markers, and numerical results (red circles) align well. The linear relationship between total pressure loss and inlet dynamic pressure confirms that losses scale proportionally with dynamic pressure, indicating no critical transitions, such as a shift from laminar to turbulent boundary layer dominate the losses within the investigated range.

Figure 8 shows the mass flow distribution measured at the outlet for the ten segments at 2xADP for the numerical (blue) and experimental (red) datasets. The numerical data demonstrate, with one exception, a relatively uniform distribution, with variations of 90-121% (one with 58%). In contrast, the experi-

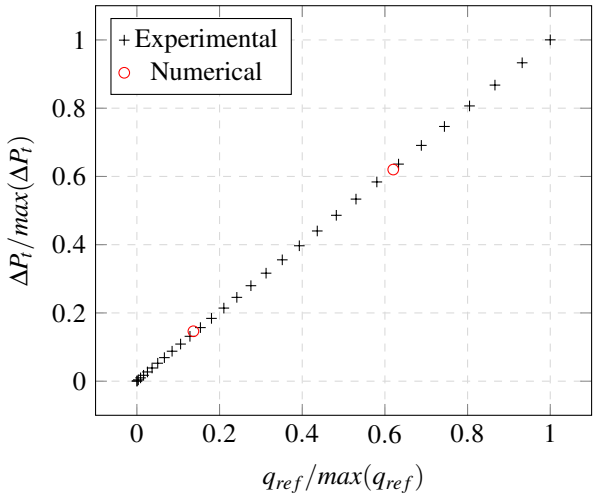

FIGURE 7. Pressure losses from the inlet to HEX outlet in relation to dynamic pressure at the inlet.

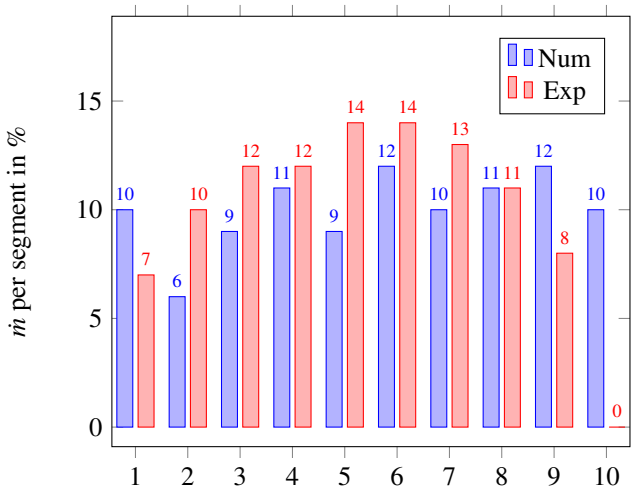

FIGURE 8. Mass flow distribution for each segment at twice the nominal (ADP); numerical (blue) and experimental (red) results

mental results, based on 12,000 data points at the outlet, reveal a significant reduction in flow in the last segment, where only 0% of the mass flow is recorded. Note that the outlet velocities are generally low, and measuring error becomes troublesome for segments with low mass flow, i.e. number 10.

The velocity magnitude from numerical results at ADP is shown in the meridional plane, together with experimental flow distribution at the outlet in figure 9. In the figure, the flow enters from the left and propagates through the domain. The guide vanes "shave-off" part of the flow for each segment, turn it through 90 degrees, then passes, mainly, radially through the tube bank before exiting at the outlet. The guide vanes form a substantial recirculation zone on the leeward side with a corresponding low-pressure zone. This forces the flow to continue to turn, in excess of 90 degrees, to flow in the opposed direction. This large re-circulating zone stretches several tube rows into the tube bank, becoming a performance inhibitor as already warm gas is brought back onto heated tubes, thereby reducing the heat transfer rate. (The opposite is true for in-flight conditions where the already cooled exhaust gas will circle back and reduce the performance of the HEX.) The size of this re-circulation zone is consequently of importance to understand and quantify - as it derates the performance of the HEX. In Fig. 9 it is clear that the size of the re-circulating zone varies between the segments, with segment two standing out as one of the worst and segment one as one of the better. Segments with a larger share of the mass flow also tend to have a larger-sized re-circulation zone. The reduction of HEX performance is however counteracted by the fact that a larger mass flow improves the heat transfer rate, albeit at a pressure loss disadvantage. The optimal solution, with uniformly radially flowing gas, is obviously, a significant challenge with a design like this. In Fig. 9 a qualitative flow distribution from the optical investigation is included. The flow distribution agrees well with the observation from the pneumatic probes in Fig.8 with nearly no flow in the 10th segment with a general increase in the middle and a notable reduction in the first.

A detailed view of segments 8 and 9 from Fig. 9 is provided in Fig. 10 with axial and radial locations of pressure taps and thermocouples illustrated, with details of the pressure distribution across two segments shown in fig. 11. In the figure the numerical and experimental results show reasonable agreement, however with a marked difference on the windward side of the baffle. These variations provide insight into the interaction between radial and axial flow components. In Fig.12 a detailed study of the pressure variation on the leeward side of the baffle is shown. In this figure, both unaltered and corrected numerical and experimental results are shown. As stated repeatedly, the mass flow distribution through the heat exchanger is crucial for its performance. In segment 8 the mass flow results from experimental and numerical matches, however slightly above the nominal at 11% In the ninth segment, however, the numerical results indicate too high a mass flow at 12% (+20%), while the experimental results significantly undershoots the mass flow at 8% (-20%). Comparing pressure loss through the tube bank with such a difference in mass flow is misleading, and hence a set of mass flow corrected data is provided in Fig. 12. Here it is assumed that the pressure loss is proportional to velocity squared. Given this correction, the predicted and measured pressure matches very well. Further studies will address and possibly find remedies to these local flow variations that make such a large impact on the flow distribution and hence performance of the HEX.

The temperature increase relative to the inlet temperature of tubes at selected axial and radial positions within segment 8 is shown in Fig.13 when the tubes are heated with constant

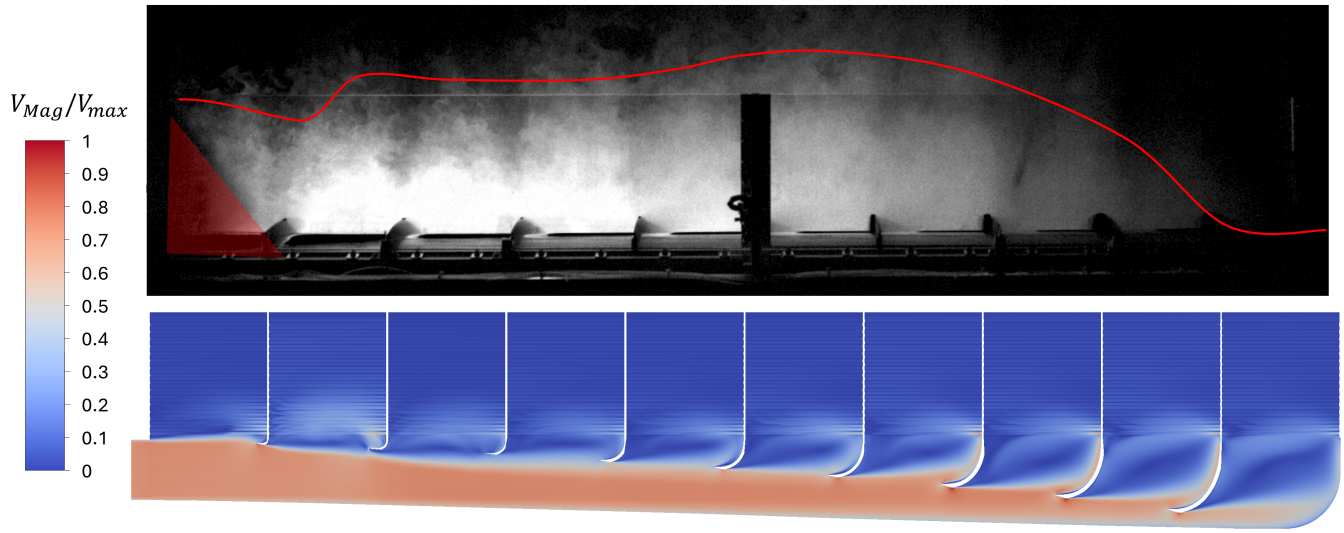

FIGURE 9. The velocity magnitude from numerical results at ADP is shown in the meridional plane, together with experimental flow distribution at the outlet. The red line indicate the average velocity and a shaded area is marked with a red triangle.

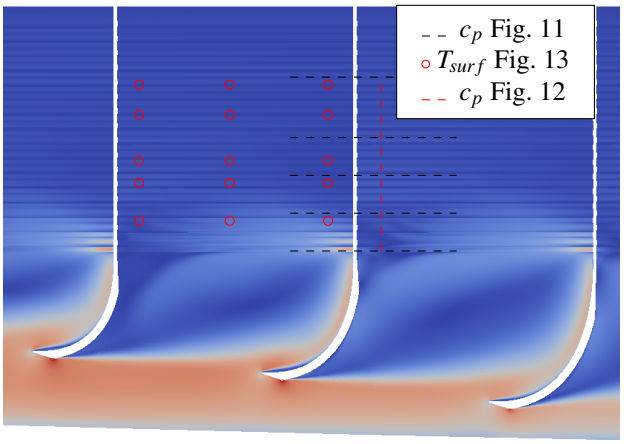

FIGURE 10. Velocity magnitude in baffle eight and nine with the location of thermocouple and pressure taps superimposed. Red markers illustrate thermocouples, dashed lines the axial movement of the pressure taps

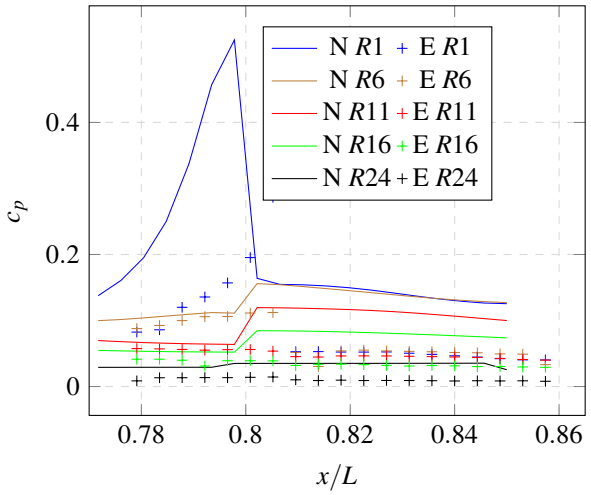

FIGURE 11. Pressure distribution along the tubes at twice the nominal (ADP) mass flow, plotted from mid segment 8 to mid segment 9 through the baffle. N for numerical results, E for experimental measurement. Rows; 1, 6, 11, 16 and 24.

input power Q. Numerical results are depicted as solid lines, while experimental thermocouple measurements are represented by dashed lines. In the current setup, a high heat transfer rate would increase cooling of the tubes and hence a drop in temperature increase of the heated tube. The agreement between CFD and experimental data is generally high, with discrepancies limited to a few percent of the total temperature difference. Beginning at row five, there is a significant axial temperature shift, with downstream temperatures showing approximately a 50% lower temperature compared to upstream locations. This phenomenon occurs due to the accelerated flow on the windward side of the baffle (axial position, x/L=0.795, see Fig. 10), which experiences a notably higher velocity and hence heat transfer rate than the conditions on the leeward side of the baffle (axial position, x/L=0.705) at the same radial location. Comparing the lowermost row (5) with the uppermost row (23), the wall temperatures show a significantly different trend. In the upstream location of these rows, the highest overall temperatures are shown,

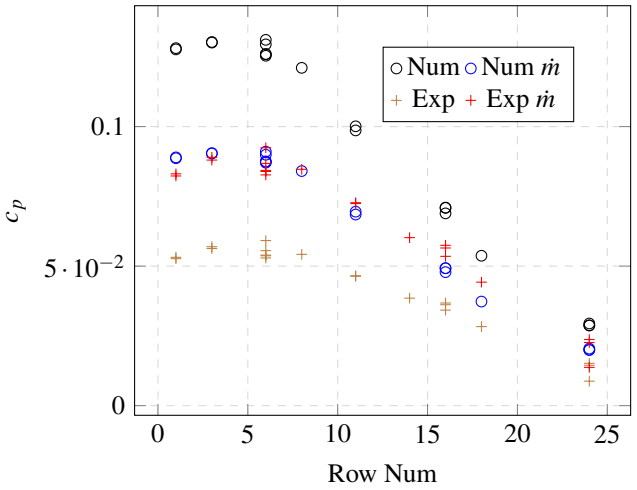

FIGURE 12. Radial pressure distribution as a function of row. Segment 9, some distance downstream (leeward position) of the baffle. Numerical (circles) and experimental (crosses), unaltered and mass flow corrected results, $\dot{m}$.

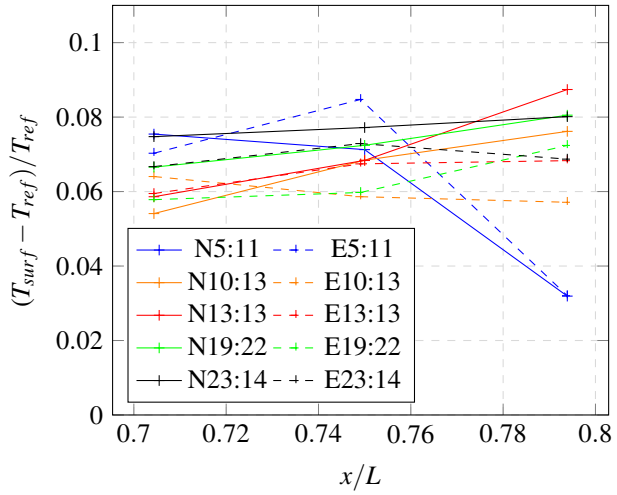

FIGURE 13. Temperature increase relative to the inlet temperature T_{ref} (vertical axis) vs. normalized axial position (horizontal axis) when heated with constant input power Q in segment 8. "N" and "E" denote numerical and experimental results, respectively, with locations as per Fig. 4; e.g., numerical values at row 5, column 11 are labeled N5:11.

indicating a low heat transfer rate, while in the downstream location, these rows give contrasting high and low temperatures, respectively. It is remarkable that both predicted and measured temperatures show the same trend and shift in magnitude of the data and occasionally matches spot on. A row 5 the accelerated flow near the downstream baffle matches well between the numerical and experimental data while the row with the largest difference between predicted and measured wall temperature is row 10. Although the data overlap, the numerically predicted results show an increasing temperature (in the axial direction), while the measured results show the opposite trend. Numerical results thus signify a larger flow redistribution within the tube bank, with a decelerated zone on the windward side of the baffle, while the measured data still indicates more uniform flow at this location. Similar trends prevails but does in general decline throughout the tube bank, with numerical results state a higher temperature, i.e. the lower velocities on the windward side of the baffle. The measured data indicate that the by row 13 the flow is fairly developed while as the while the slope persist for numerical data up to row 19. As the flow progresses through the domain, the temperature distribution within segment 8 becomes increasingly uniform.

6 Conclusion

This work evaluates the airside performance of a heat recovery heat exchanger (HEX) for the WET cycle, where numerical and experimental results show strong agreement of overall aerodynamic and thermodynamic performance. Traditional HEX studies can often assume uniform inlet flow and treat heat exchangers as black boxes, relying primarily on energy balance. However, such an assumption is not suitable for the current setup, where non-uniformity and recirculation significantly influence HEX performance. This study examines flow phenomena in detail, identifying discrepancies in flow distribution and heat transfer when assessing HEX performance at a more detailed scale.

A key finding is the role of flow turning and non-uniform flow distribution for a heat exchanger performance even though total pressure losses over the domain is matching well. The 90-degree redirection of exhaust gases results in highly non-uniform flow distribution between the segments and with localized pressure variations propagating into the tube bank. A detailed analysis of segments eight and nine reveals that total pressure losses align well between numerical and experimental results when adjusted for mass flow differences between the segment. However, internal flow structure deviates significantly, with differences in the effect and propagation into the HEX. Numerical results suggest that these propagate as long as row 19 (of 32) while experimental suggest until 10. It is likely that the discrepancies would be less if the flow was more uniformly distributed as the effects are particularly noticeable near the baffles and guide vanes.

The results emphasize the importance of integrating numerical and experimental approaches to capture both global performance trends and localized deviations. The detailed numerical modeling, utilizing a 65-million-cell computational domain, successfully resolves key heat transfer characteristics. However, a sub-model was required to accurately correlate numerical and experimental results. Furthermore, traditional liquid-based heating methods were deemed unsuitable for the current configuration, and Kanthal wires have been demonstrated to provide a reliable and high-resolution heat flux characterization for long and thin tubes with unknown heat flux distributions.

From a design perspective, these findings provide critical in-

put for future heat exchanger configurations and highlight the importance of experimental validation under engine-representative conditions. Even relatively simple experimental setups can uncover key flow behaviors that are not fully captured in numerical models.

Ultimately, these differences highlight the complexity of predicting heat transfer and pressure losses in a turning, non-uniform flow environment, a challenge that has been and is expected to persist in aviation applications involving high thermal flow, such as many future sustainable engine concepts.

Contribution

J.Br. performed numerical calculations and analysis, managed the overall project, and contributed to manuscript preparation. I.J. provided the experimental concept, developed the experimental setup, and contributed to the manuscript writing. V.V. carried out the majority of the experimental evaluation and data analysis. Y.A. contributed with (CFD) simulations. J.Br. and I.J. led the writing and refinement of the manuscript, with all authors discussing and reviewing the manuscript.

ACKNOWLEDGMENT

Funded by the European Union. Views and opinions expressed are however those of the author(s) only and do not necessarily reflect those of the European Union or Clean Aviation Joint Undertaking. Neither the European Union nor the granting authority can be held responsible for them. The project is supported by the Clean Aviation Joint Undertaking and its members. This project has received funding from the Clean Aviation Joint Undertaking under the European Union's Horizon Europe research and innovation program (Grant Agreement no. 101102006). The authors also acknowledge the support provided by the department of Mechanics and Maritime Sciences at Chalmers University of Technology. Additional funding is provided by GKN Aerospace Sweden AB.

REFERENCES

[1] Rolt, A., and Baker, N. J., 2009. "Intercooled turbofan engine design and technology research in the eu framework 6 newac programme".

[2] Kwan, P.-W., and et al., 2011. "Minimising loss in a heat exchanger installation for an intercooled turbofan engine". Vol. Volume 1: Aircraft Engine; Ceramics; Coal, Biomass and Alternative Fuels; Wind Turbine Technology of *Turbo Expo: Power for Land, Sea, and Air*, pp. 189–200.

[3] Poutriquet, F., von der Bank, R., Bourgeois, S., Tantot, N., Donnerhack, S., Lundblath, A., Peschiulli, A., Basset, E., Guin, C., Hassa, C., and Gebel, G. C., 2016. "Lemcotec : a key project to tackle pollutant emissions by developing new core technologies.". In Greener Aviation 2016, C. Mari and V. Guénon, eds., pp. 27–1.

[4] Zhao, X., 2016. "Aero engine intercooling". PhD thesis, Chalmers University of Technology.

[5] Hentati, A., Mlika, Z., Frigon, J.-F., and Ajib, W., 2022. "Energy harvesting wireless sensor networks: Inter-delivery-aware scheduling algorithms". In 2022 IEEE Wireless Communications and Networking Conference (WCNC), pp. 1135–1139.

[6] Misirlis, D., Vlahostergios, Z., Flouros, M., Salpingidou, C., Donnerhack, S., Goulas, A., and Yakinthos, K., 2017. "Optimization of heat exchangers for intercooled recuperated aero engines". *Aerospace,* ***4***(1).

[7] Alexandre, C. P., Jonsson, I., Xisto, C., Lundbladh, A., and Grönstedt, T., 2024. "Compact heat exchangers for hydrogen-fueled aero engine intercooling and recuperation". *Applied Thermal Engineering,* ***243***, p. 122538.

[8] Cheng, D. Y., U.S. Patent 3,978,661, 1976. Parallel-compound dual-fluid heat engine.

[9] Cheng, D. Y., U.S. Patent 4,128,994, 1978. Regenerative parallel compound dual-fluid heat engine.

[10] ARPA-E, 2022. Hydrogen steam and inter-cooled turbine engine (hysite). ARPA-E, US Goverment of Energy. Last accessed: 03/06/2022.

[11] Kaiser, S., Schmitz, O., Ziegler, P., and Klingels, H., 2022. "The water-enhanced turbofan as enabler for climate-neutral aviation". *Appl. Sci.,* ***12***, p. 12431.

[12] VDI-Gesellschaft Verfahrenstechnik und Chemieingenieurwesen (GVC), E., 2010. *VDI Atlas*. Springer-Verlag Berlin Heidelberg.

[13] Vikhorev, V., Chernoray, V., Mallak, Z. A., and Larsson, J., 2022. "The influence of the vane lean on the flow in a turbine rear structure". In Congress of the International Council of the Aeronautical Sciences (ICAS).

[14] International Organization for Standardization (ISO), 2003. Iso 5167 - measurement of fluid flow by means of pressure differential devices inserted in circular cross-section conduits running full. International Standard 5167, ISO, Geneva, Switzerland.

[15] American Society of Mechanical Engineers (ASME), 2020. Ptc 19.1 - test uncertainty. Performance Test Code 19.1, ASME, New York, NY, USA.

[16] Menter, F. R., 1994. "Two-equation eddy-viscosity turbulence models for engineering applications". *AIAA Journal,* ***32***(8), pp. 1598–1605.